ANNUAL REPORT

on

FAILURE CRITERIA IN LAMINATES BASED ON 3D MICROMECHANIC CONSIDERATIONS

by:

E.S. Folias

Submitted to

AIRFORCE OFFICE OF SCIENTIFIC RESEARCH

Department of Mechanical Engineering
University of Utah
Salt Lake City, Utah 84112

August , 1991

ON THE THREE-DIMENSIONAL STRESS FIELD OF A PERIODIC ARRAY OF FIBERS EMBEDDED INTO A PLATE MATRIX [1]

by
E.S. Folias and J.H. Liu

Department of Mathematics
University of Utah
Salt Lake City, Utah 84112

[1]This work was supported in part by the Air Force Office of Scientific Research Grant No. AFOSR-87-0204. The author wishes to thank Lt. Col. G. Haritos for this support and for various discussions

Abstract

A 3D micromechanical model has been developed to represent a undirectional composite plate which is subjected to a uniform transverse load σ_o. The model assumes the fibers to be cylindrical inclusions which are periodically embedded into an epoxy matrix. The materials of both fibers and matrix are assumed to be linear, elastic, and isotropic. The analytical solution shows the radial stress σ_{rr} to decrease as the fiber volume fraction V_f increases. The stress profile along a fiber length is shown to be constant except in the neighborhood of the fiber edge where a boundary layer is shown to prevail. In this region, the analytical solution shows the stress field to be singular which is a departure from the results given by macromechanical theories.

In the limit, as $G_f \rightarrow 0^+$ the 3D stress field of a plate weakened by a periodic array of holes is recovered.

1 INTRODUCTION

It is well recognized that fiber composite materials are very attractive for use in aerospace, automotive and other applications. These composites consist of relatively stiff fibers which are embedded into a lower stiffness matrix. Although in most designs the fibers are aligned so that they are parallel to the direction of the external loads, it is almost impossible to avoid induced transverse stresses which may lead to premature failure of the laminate. An excellent example of this is the case of a filament wound pressure vessel in which the presence of curvature induces bending as well as transverse stresses (Folias, 1965). However, in order to be able to predict their failing characteristics, particularly in the neighborhood of free surfaces such as holes, edges etc., it is necessary to know the local stress behavior from a 3D point of view.

An overall summary of some of the results, which are based on 2D elasticity considerations can be found in the books by Hull (1981) and by Chamis (1975). In their pioneering work, Adams and Doner (1967) used finite differences to solve the problem of a doubly periodic array of elastic fibers contained in an elastic matrix and subjected to a transverse load. Their results reveal the dependence of the maximum principal stress versus the constituent stiffness ratio (E_f/E_m) for various fiber volume ratios. A

few years later, Yu and Sendeckyj (1974) used a complex variable approach to solve the problem of multiple inclusions embedded into an infinite matrix. Their results were subsequently specialized to cases of two and three inclusions thus providing us with further insight into the strength of the composite.

In this paper, we will construct an analytical solution for the 3D stress field of a matrix which has been reinforced in one of the directions with cylindrical fibers.

2 Formulation of the problem

Consider the equilibrium of a body which occupies the space $|x| < \infty, |y| < \infty, |z| \leq h$ and contains a periodic array of cylindrical inclusions of radius a, whose generators are parallel to the z-axis (see Fig. 1). The physical situation depicted here is that of a uniderectional composite plate that consists of a matrix where fibers are embedded into. For convenience, all quanties with the script (m) will refer to the matrix while quanties the with script f will refer to the fibers. The materials of both matrix and fibers will be assumed to be homogeneous, isotropic and linear elastic. At the interface, i.e. at $r = a$, perfect bonding will be assumed to prevail. As to loading, a uniform tensile stress σ_o is applied on the composite plate (see Fig. 1) which is in a direction perpendicular to the axis of the fibers. Furthermore, the surface $|z| = h$, for both regions, matrix and inclusion, will be assumed to be free of stress and constraints.

In the absence of body forces, the coupled differential equations governing the displacement functions $u_i^{(j)}$ are :

$$\frac{1}{1-2\nu_j}\frac{\partial e^{(j)}}{\partial x_i} + \nabla^2 u_i^{(j)} = 0; \quad i = 1,2,3; \; j = m, f \tag{1}$$

where ∇^2 is the Laplacian operator, ν_j is Poisson's ratio, $u_i^{(m)}$ and $u_i^{(f)}$ represent the displacement functions in the matrix and fibers respectively, and

$$e^{(j)} = \frac{\partial u_i^{(j)}}{\partial x_i} \;\; ; \;\; i = 1,2,3 \;\; ; \;\; j = m, f. \tag{2}$$

The stress-displacement relations are given by Hooke's law as

$$\sigma_{ik}^{(j)} = \lambda_j e_{ll}^{(j)} \delta_{ik} + 2G_j e_{ik}^{(j)} \tag{3}$$

where λ_j and G_j are the Lame constants describing the material properties of the matrix and of the inclusions.

As to boundary conditions, one must require that (see Fig. 2 for cell configuration)

$$at \qquad |z| = h: \qquad \sigma_{zz}^{(j)} = \tau_{xz}^{(j)} = \tau_{yz}^{(j)} = 0; \quad j = m, f. \tag{4}$$

$$at \qquad r = a: \quad u_r^{(m)} - u_r^{(f)} = u_\theta^{(m)} - u_\theta^{(f)} = u_z^{(m)} - u_z^{(f)} = 0. \tag{5}$$

$$\sigma_{rr}^{(m)} - \sigma_{rr}^{(f)} = \tau_{r\theta}^{(m)} - \tau_{r\theta}^{(f)} = \tau_{rz}^{(m)} - \tau_{rz}^{(f)} = 0 \tag{6}$$

Moreover, at $r = 0$ we require that all stresses and displacements be finite. the cell configuration boundaries AB and CD will be taken as planes of symmetry, thus satisfying the respective boundary conditions automatically. It remains, therefore, for us to satisfy only the continuity boundary conditions along the segment BC, i.e.

$$u_x^{(m)}(\theta) - u_x^{(m)}(\frac{\pi}{4}) = -u_x^{(m)}(\frac{\pi}{2} - \theta) + u_x^{(m)}(\frac{\pi}{4}) \tag{7}$$

$$u_y^{(m)}(\theta) - u_y^{(m)}(\frac{\pi}{4}) = -u_y^{(m)}(\frac{\pi}{2} - \theta) + u_y^{(m)}(\frac{\pi}{4}) \tag{8}$$

$$F_x^{(m)}(\theta) = F_x^{(m)}(\frac{\pi}{2} - \theta) \tag{9}$$

$$F_y^{(m)}(\theta) = F_y^{(m)}(\frac{\pi}{2} - \theta). \tag{10}$$

Fianlly, in order to complete the formulation of the problem, one must also require the resultant forces

$$\int_{BC} F_x ds = 0 \tag{11}$$

$$\int_{BC} F_y ds = b\sigma_o. \tag{12}$$

It is found convenient at this stage to seek the solution to equation (1) in the form:

$$u_i^{(j)} = u_i^{(p)(j)} + u_i^{(c)(j)} \; ; \; i = 1,2,3; \; j = m, f \tag{13}$$

where the first term represents the particular solution and the second term the complementary solution.

3 Method of Solution

A generalized analytical solution to a class of three-dimensional problems which arise in elastostatics has been constructed by Folias (1975 , 1990a). The solution was subsequently used, Folias and Wang (1990b), to solve for the 3D stress field in a plate which has been weakened by a hole. This work was later extended to the solution of an isotropic inclusion embedded into a matrix, Penado and Folias (1989). On the bases of these results, one may now assume the solution to system (1), which automatically satisfies the boundary conditions at the plate faces eq. (4), in the form [2] :

$$\begin{aligned} u^{(c)(j)} = & \frac{1}{m_j - 2} \sum_{\nu=1}^{\infty} \frac{\partial^2 H_\nu^{(j)}}{\partial x^2} \{2(m_j - 1) f_1(\beta_\nu z) + m_j f_2(\beta_\nu z)\} \\ & + \sum_{n=1}^{\infty} \left\{ -\frac{\partial^2 H_n^{(j)}}{\partial x^2} + \alpha_n^2 H_n^{(j)} \right\} cos\ (\alpha_n h)\ cos\ (\alpha_n z) \\ & + \lambda_1^{(j)} - y \frac{\partial \lambda_3^{(j)}}{\partial x} + \frac{1}{m_j + 1} z^2 \frac{\partial^2 \lambda_3^{(j)}}{\partial x \partial y} \end{aligned} \tag{14}$$

$$v^{(c)(j)} = \frac{1}{m_j - 2} \sum_{\nu=1}^{\infty} \frac{\partial^2 H_\nu^{(j)}}{\partial x \partial y} \{2(m_j - 1) f_1(\beta_\nu z) + m_j f_2(\beta_\nu z)\}$$

[2] Note that because of symmetry in the present problem, one needs only to consider the region $0 \leq \theta \leq \pi|2$.

$$-\sum_{n=1}^{\infty}\frac{\partial^2 H_n^{(j)}}{\partial x\partial y}\,cos\,(\alpha_n h)\,cos\,(\alpha_n z) \tag{15}$$

$$+\frac{3m_j-1}{m_j+1}\lambda_3^{(j)}+\lambda_2^{(j)}-y\frac{\partial\lambda_3^{(j)}}{\partial y}-\frac{1}{m_j+1}z^2\frac{\partial^2\lambda_3^{(j)}}{\partial x^2}$$

$$w^{(c)(i)}=\frac{1}{m_j-2}\sum_{\nu=1}^{\infty}\frac{\partial H_\nu^{(j)}}{\partial x}\beta_\nu\left\{(m_j-2)f_3(\beta_\nu z)-m_j f_4(\beta_\nu z)\right\}-\frac{1}{m_j+1}z\frac{\partial\lambda_3^{(j)}}{\partial y} \tag{16}$$

From which the stresses can easily be obtained as:

$$\frac{1}{2G_j}\sigma_{xx}^{(c)(j)}=\frac{1}{m_j-2}\sum_{\nu=1}^{\infty}\left\{2\beta_\nu^2\frac{\partial H_\nu^{(j)}}{\partial x}f_1(\beta_\nu z)\right.$$

$$\left.+\frac{\partial^3 H_\nu^{(j)}}{\partial x^3}[2(m_j-1)f_1(\beta_\nu z)+m_j f_2(\beta_\nu z)]\right\} \tag{17}$$

$$+\sum_{n=1}^{\infty}\left\{-\frac{\partial^3 H_n^{(j)}}{\partial x^3}+\alpha_n^2\frac{\partial H_n^{(j)}}{\partial x}\right\}\,cos\,(\alpha_n h)\,cos\,(\alpha_n z)$$

$$+\frac{\partial\lambda_1^{(j)}}{\partial x}-y\frac{\partial^2\lambda_3^{(j)}}{\partial x^2}+\frac{2}{m_j+1}\frac{\partial\lambda_3^{(j)}}{\partial y}+\frac{1}{m_j+1}z^2\frac{\partial^3\lambda_3^{(j)}}{\partial x^2\partial y}$$

$$\frac{1}{2G_j}\sigma_{yy}^{(c)(j)}=\frac{1}{m_j-2}\sum_{\nu=1}^{\infty}\left\{2\beta_\nu^2\frac{\partial H_\nu^{(j)}}{\partial x}f_1(\beta_\nu z)\right.$$

$$\left.-(\frac{\partial^3 H_\nu^{(j)}}{\partial x^3}-\beta_\nu^2\frac{\partial H_\nu^{(j)}}{\partial x})[2(m_j-1)f_1(\beta_\nu z)+m_j f_2(\beta_\nu z)]\right\} \tag{18}$$

$$+\sum_{n=1}^{\infty}\left\{\frac{\partial^3 H_n^{(j)}}{\partial x^3}-\alpha_n^2\frac{\partial H_n^{(j)}}{\partial x}\right\}\,cos\,(\alpha_n h)\,cos\,(\alpha_n z)$$

$$+\frac{2m_j}{m_j+1}\frac{\partial\lambda_3^{(j)}}{\partial y}-\frac{\partial\lambda_1^{(j)}}{\partial x}+y\frac{\partial^2\lambda_3^{(j)}}{\partial x^2}-\frac{1}{m_j+1}z^2\frac{\partial^3\lambda_3^{(j)}}{\partial x^2\partial y}$$

$$\frac{1}{2G_j}\sigma_{zz}^{(c)(j)} = -\frac{m_j}{m_j-2}\sum_{\nu=1}^{\infty}\frac{\partial H_\nu^{(j)}}{\partial x}\beta_\nu^2 f_2(\beta_\nu z) \tag{19}$$

$$\frac{1}{2G_j}\tau_{xy}^{(c)(j)} = \frac{1}{m_j-2}\sum_{\nu=1}^{\infty}\frac{\partial^3 H_\nu^{(j)}}{\partial x^2\partial y}\{2(m_j-1)f_1(\beta_\nu z)+m_j f_2(\beta_\nu z)\}$$

$$-\sum_{n=1}^{\infty}\left\{\frac{\partial^3 H_n^{(j)}}{\partial x^2\partial y}-\frac{1}{2}\alpha_n^2\frac{\partial H_n^{(j)}}{\partial y}\right\}\cos(\alpha_n h)\cos(\alpha_n z) \tag{20}$$

$$+\frac{m_j-1}{m_j+1}\frac{\partial\lambda_3^{(j)}}{\partial x}+\frac{\partial\lambda_2^{(j)}}{\partial x}-y\frac{\partial^2\lambda_3^{(j)}}{\partial x\partial y}-\frac{1}{m_j+1}z^2\frac{\partial^3\lambda_3^{(j)}}{\partial x^3}$$

$$\frac{1}{2G_j}\tau_{yz}^{(c)(j)} = -\frac{m_j}{m_j-2}\sum_{\nu=1}^{\infty}\frac{\partial^2 H_\nu^{(j)}}{\partial x\partial y}\beta_\nu\{f_3(\beta_\nu z)+f_4(\beta_\nu z)\}$$

$$+\frac{1}{2}\sum_{n=1}^{\infty}\alpha_n\frac{\partial^2 H_n^{(j)}}{\partial x\partial y}\cos(\alpha_n h)\sin(\alpha_n z) \tag{21}$$

$$\frac{1}{2G_j}\tau_{xz}^{(c)(j)} = -\frac{m_j}{m_j-1}\sum_{n=1}^{\infty}\frac{\partial^2 H_\nu^{(j)}}{\partial x^2}\beta_\nu\{f_3(\beta_\nu z)+f_4(\beta_\nu z)\}$$

$$+\frac{1}{2}\sum_{n=1}^{\infty}[\frac{\partial^2 H_n^{(j)}}{\partial x^2}-\alpha_n^2 H_n^{(j)}]\alpha_n\cos(\alpha_n h)\sin(\alpha_n z), \tag{22}$$

where

$$\alpha_n = \frac{n\pi}{h}, n = 1,2,3,\ldots, \tag{23}$$

β_ν are the roots of the equation

$$\sin(2\beta_\nu h) = -(2\beta_\nu h), \tag{24}$$

$H_\nu^{(j)}$ and $H_n^{(j)}$ are functions of x and y which satisfy the reduced wave equation:

$$(\frac{\partial^2}{\partial x^2}+\frac{\partial^2}{\partial y^2}-\beta_\nu^2)\frac{\partial H_\nu^{(j)}}{\partial x} = 0 \tag{25}$$

$$(\frac{\partial^2}{\partial x^2} + \frac{\partial^2}{\partial y^2} - \alpha_n^2)\frac{\partial H_n^{(j)}}{\partial y} = 0 \tag{26}$$

$\lambda_1^{(j)}, \lambda_2^{(j)}$ and $\lambda_3^{(j)}$ are two dimensional harmonic functions, and

$$f_1(\beta_\nu z) \equiv \ cos\ (\beta_\nu h)\ cos\ (\beta_\nu z) \tag{27}$$

$$f_2(\beta z) \equiv \beta_\nu h\ sin\ (\beta_\nu h)\ cos\ (\beta_\nu z) - \beta_\nu z\ cos\ (\beta_\nu h)\ sin\ (\beta_\nu z) \tag{28}$$

$$f_3(\beta_\nu z) \equiv \ cos\ (\beta_\nu h)\ sin\ (\beta_\nu z) \tag{29}$$

$$f_4(\beta_\nu z) \equiv \beta_\nu h\ sin\ (\beta_\nu h)\ sin\ (\beta_\nu z) + \beta_\nu z\ cos\ (\beta_\nu h)\ cos\ (\beta_\nu z). \tag{30}$$

Examining the nature of the boundary conditions, we furthermore construct the solution to equations (25) and (26) in the form:

$$H_\nu^{(m)} = \sum_{k=0}^{\infty} a_k K_k(\beta_\nu r)\ cos\ (2k\theta) \tag{31}$$

$$H_\nu^{(f)} = \sum_{k=0}^{\infty} b_k I_k(\beta_\nu r)\ cos\ (2k\theta) \tag{32}$$

$$H_n^{(m)} = \sum_{k=0}^{\infty} C_k K_k(\alpha_n r)\ sin\ (2k\theta) \tag{33}$$

$$H_n^{(f)} = \sum_{k=0}^{\infty} d_k I_k(\alpha_n r)\ sin\ (2k\theta). \tag{34}$$

$$\lambda_1^{(m)} = \sum_{k=0}^{\infty} (-1)^k \frac{A_k}{r}\ sin\ (2k+1)\theta \tag{35}$$

$$\lambda_2^{(m)} = \sum_{k=0}^{\infty} (-1)^k \frac{A_k}{r}\ cos\ (2k+1)\theta \tag{36}$$

$$\lambda_3^{(m)} = \sum_{k=0}^{\infty} (-1)^k \frac{B_k}{r}\ cos\ (2k+1)\theta \tag{37}$$

$$\lambda_1^{(f)} = \sum_{k=0}^{\infty} (-1)^k E_k r \; sin \; (2k+1)\theta \tag{38}$$

$$\lambda_2^{(f)} = \sum_{k=0}^{\infty} (-1)^k E_k r \; cos \; (2k+1)\theta \tag{39}$$

$$\lambda_3^{(f)} = \sum_{k=0}^{\infty} (-1)^k G_k r \; cos \; (2k+1)\theta \tag{40}$$

where $I_k(\beta r)$ and $K_k(\beta r)$represent the modified Bessel functions of the first and second kind and $a_k, b_k, c_k, d_k, A_k, B_k, E_k$ and G_k are arbitrary constants to be determined from the remaining boundary conditions (5) - (12). Upon substitution of equations (14) - (40) into equations (5) - (12) one arrives at a system of twelve equations involving series in z. The system may then be solved numerically for the unknown coefficients. Perhaps it may be worth noting that in our numerical analysis we satisfied first the boundary conditions at $r = a$ by using well over 200 roots. The method of solution, as well as the rate of convergence of these series, is similar to that found by Penado and Folias (1989, see reference for details). The system is sensitive to small changes and for this reason double precision was used throughout the numerical analysis.

4 Numerical results

Once the coefficients have numerically been determined, the stresses and displacements may then be calculated at any point in the body. Avoiding the long and tedious numerical details, the behavior of the stresses σ_{rr} and $\sigma_{\theta\theta}$ versus (z/h) and at $r = a$ and $\theta = 0$ are given by figures 3 and 4 respectively. It is noted that the stresses along the interior length of the fiber are essentially constant and that as one approaches the edge of the fiber length, a boundary layer is shown to exist. This sudden change suggests, therefore, the presence of a stress singularity at such regions. Indeed, a separate asymptotic analysis for the investigation of the local stress field, at such neighborhoods, shows the stresses to be proportional to $\rho^{-\alpha}$, where $\alpha = 0.249$ for a glass fiber/epoxy matrix interface (Folias 1989) and $\alpha = 0.318$ for a carbon fiber [3]/ epoxy matrix interface (Li and Folias 1990). It may also be noted that Figs 3 and 4 provide us with important information concerning the regions of applicability of macromechanical theories. The reader may recall that such theories predict the stress values at edges to be finite, except in the vicinity of an interface where the singularity strength is shown to be very weak (Wang and Choi, 1982; Folias, 1991). Thus, they tend to underestimate the actual stress levels at such edges, e.g. surface of a hole, surface of a crack etc. But, if one is to study damage evolution at such regions, the knowledge of the local stress field is essential. Be that as it may, a closer examination of Figs 3 and 4 shows the boundary layer region, for a transverse applied load, to be restricted to a distance of one fiber diameter away from the fiber edge. On the other hand, if the applied load is in the direction of the fiber axis, the boundary layer is then spread out to a distance of six fiber diameters away from the edge (Zhong and Folias 1991). Thus coupling between the macromechanical and micromechanical results may be desirable in predicting local damage due to fracture.

Returning to the stress profiles σ_{rr} and $\sigma_{\theta\theta}$ (Fig. 3 and 4) we note that the magnitude of the stresses decreases as the fiber volume fraction, V_f, increases. The decrease, however, is only noticed when the spacing of the fibers becomes less than four fiber diameters center to center. Figs 5 and 6 show typical stress profiles for σ_{rr} and $\sigma_{\theta\theta}$ as a function of G_f/G_m. It

[3] In this analysis the material of the carbon fiber is assumed to be transversely isotropic.

is interesting to note that the circumferencial stress $\sigma_{\theta\theta}$ decreases rapidly as the ratio (G_f/G_m) increases. For glass fiber/epoxy matrix $(G_f/G_m) = 16.67$, which implies that the $\sigma_{\theta\theta}$ stress is approximately zero. Thus, all things being equal, the controlling stress for possible crack failure is the radial stress σ_{rr} at the particular location of $\theta = 0$. For large (G_f/G_m) ratios, the radial stress reaches an asymptotic value. A similar result was also obtained by other researchers based on 2D considerations (e.g. Adams and Donen 1967). In Fig. 7, a plot of the radial stress on the interface boundary is shown to decrease as the angle θ increases. On the other hand, the shear stress $\tau_{r\theta}$ (See Fig. 8) vanishes at the two positions $\theta = 0°$ and 90° and attains its maximum value at $\theta \approx 45°$. The location of this maximum shifts slightly to the right as the ratio of (a/b) increases. Similar stress profiles also appear as one moves towards the free surface. At the free surface, the question arises as to whether the strength of the stress singularity is affected as the separation distance between fibers becomes smaller and smaller. While initially the authors believed that this may be the case, lately they believe that the singularity strength will not be altered but that the function multiplying the singular term is expected to change. Be that as it may, the subject is under further investigation.

5 Conclusions

A 3D micromechanical model has been developed to represent the response of a unidirectional composite plate subject to a transverse load. In this model, the fibers are considered to be cylindrical inclusions which are periodically embedded into the matrix. The material of both fibers and matrix is assumed to be linear, elastic and isotropic. The analysis has shown that, as the fiber volume fraction V_f increases, the radial stress σ_{rr} decreases by 30 to 40 percent. On the other hand, the circumferential stress $\sigma_{\theta\theta}$ is almost negligible. The stress profiles across the fiber length are almost constant except in the neighborhood of the fiber edge, where a boundary layer is shown to prevail. In this region, the stress field possesses a weak stress singularity which for a glass fiber/epoxy matrix composite is of the order 0.25. This result represents a departure from the results predicted by a macromechanical theory. This inconsistency is attributed to the fact that macromechanical theories tend to average the local effects throughout each

layer thickness, and as a result all stresses at the edge are predicted to be finite. Thus, the present analysis also provides us with important information regarding the regions of applicability of macromechanical theories.

A closer examination of the stress field reveals that, in the presence of a crack, the damaging stress for possible failure is the radial stress σ_{rr}, particularly at the location $\theta = 0$. Two types of failure immediately come to mind: a fiber/matrix interface crack and a radial matrix crack. In conjunction with this work, the former was recently considered by Folias (1991) and the latter by Folias and Liu (1991).

It is well recognized that void nucleation occurs more readily in a triaxial tensile stress field, a result which is consistent with experimental observations. Such a model for estimating the void nucleation stress may now be obtained, if in our previous analysis we let $G_f \to 0^+$. The physical situation depicted here is that of a matrix which has been weakened by a uniformly distributed periodic array of cylindrical voids or holes. Such an estimate may then serve as a lower bound for the transverse strength of a unidirectional composite plate. Without going into the numerical details, we plot in Fig. 9 the stress concentration factor $\sigma_{\theta\theta}$ through the thickness (z/h) and for a typical ratio of $(a/b) = 0.3$. It is noted that the s.c.f. is relatively constant throughout the interior and that it rises slightly as it reaches the vicinity of the free surface whereby it begins to drop rather abruptly. The characteristic stress profile is in agreement with that found by Folias and Wang (1990) for the case of one hole. the variation of the s.c.f. as a function of the ratio (a/b) is given by Fig. 10, where it may be noted that the void volume fraction in the matrix is given by

$$V_h = (\frac{\pi}{2})(\frac{a}{b})^2. \tag{41}$$

It is clear from this Fig. that the s.c.f. increases rather rapidly as the void volume fraction ratio increases. The result is in agreement with our physical expectations. A similar stress profile is also observed throughout the thickness including the plane [4] $z = h$. (see Fig. 11). Finally, in Figs. 12a and 12b we plot the variation of the s.c.f. on the planes $z = 0$ and $z = h$ as a function of the position angle θ and for different (a/b) ratios.

[4] Folias (1987) has shown that no stress singularity is present in the vicinity of the intersection of the hole surface and the free of stress plane.

It is noted that in the region $70° < \theta < 90°$ the s.c.f. is relatively flat. This is the region where a crack is most likely to initiate and subsequently propagate.

It is now possible for us to develop approximate fracture criteria for the prediction of the transverse tensible strength. For example, let us consider the case of an epoxy matrix which has been weakened by the presence of a periodic array of cylindrical holes. The situation depicted here is that of a composite in which every fiber/matrix interface is debonded. From a practical point of view, the transverse strength of such a case may serve as a lower bound estimate to the composite. Thus, if we assume that a radial crack has developed at the edge of one of the holes (see Fig. 13), then the following approximate criterion for crack initiation may be used[5]:

$$\left\{\frac{3.10 \quad \sigma_o}{3.00 \quad \Psi(V_h)}\right\} \sqrt{\pi c} F(\frac{c}{a_h}) \approx 2\sqrt{\frac{\gamma_m G_m}{1-\nu_m}}, \tag{42}$$

where the function Ψ is given by Fig. 14 and the function $F(\frac{c}{a_h})$ is given by the table below (See Hellan 1984, p.246).

Table 1

$(\frac{c}{a_h})$	0.00	0.10	0.20	0.30
$F(\frac{c}{a_h})$	3.36	2.73	2.30	2.04

Assuming next a crack length of $0.10a_h$ and an epoxy matrix with the properties:

$$\begin{array}{ll} G_m = 2.10Gpa & \nu_m = 0.34 \\ 2\gamma_m = 123\frac{J}{m^2} & 2a_h = 10^{-3}m \\ (\frac{a}{h}) = 0.05 & V_h = 0.357 \end{array}$$

one finds

$$(\sigma_o)_r \approx 24.39\ Mpa \approx 3.54ksi. \tag{43}$$

[5]The 3.10 factor is due to the triaxility effect (see Fig. 9) which is applicable to $(a/h) = 0.05$, thus a conservative value. Also, the equation is valued for all $-h < z < h$.

This value may now be thought of as a lower bound estimate of the transverse strength in a unidirectional composite plate. In practice, an examination of the material will provide the size of a typical hole diameter to be used in the above analysis. The criterion may also be used in reverse in order to establish material specifications.

In closing, it may be appropriate here to note that the analysis may now be extended to also include row of fibers with different fiber orientations, which points to the concept of a laminated composite plate. This defines the subject of a subsequent paper.

References

Adams, D.F. and Doner, D.R., 1967, "Transverse Normal Loading of a Unidirectional Composite", J. of Composite Mateirals, Vol. 1, pp.152-164.

Chamis, C.C., 1975, Edited, "Composite Materials", Academic Press, Vol. 1-8.

Folias, E.S., 1989, "The 3D Stress Singularities at the Intersection of a Cylindrical Inclusion and a Free Surface", International Journal of Fracture, Vol. 39, pp. 25-34

Folias, E.S., 1987, "The 3D Stress Field at the Intersection of a Hole and a Free Surface", International Journal of Fracture, Vol. 35, No. 3, pp. 187-194.

Foilias, E.S., "A 3D Griffith Criterion for the Prediction of Failures in Plates Weakened by a Hole" under review, Journal of Applied Mechanics.

Folias, E.S. and Liu, J., 1990, "The 3D Stress Field of a Cylindrical Fiber Embedded into a Matrix with a Layer of Modified Matrix Around the Fiber" under review.

Folias, E.S. and Reuter, W., 1990, "A General 3D Analytical Solution for the Equilibrium of Linear Elastic Plates" International Journal of Computational Mechanics, Vol. 5, pp. 459-468.

Folias, E.S. and Wang, J.J., 1990, "On the Three-Dimensional Stress Field Around a Circular Hole in a Plate of an Arbitrary Thickness", Computational Mechanics, Vol. 6, No. 5.

Hull, D., 1981, "An Introduction to Composite Materials", Cambridge University Press.

Li, P.C. and Folias, E.S., "The 3D Stress Field of a Carbon Fiber Intersecting a Free Surface and Under the Action of a Uniform Transverse Load", in press, International Journal of Mechanics of Materials.

Penado, F.E.; Folias, E.S., 1989, "The Three-Dimensional Stress Field Around a Cylindrical Inclusion in a Plate of Arbitrary Thickness", International Journal of Fracture, Vol. 39, pp. 129-146.

Yu, I.W. and Sendeckyj, G.P., 1974, "Multiple Circular Inclusion Problems in Plane Elastostatics," pp. 215-220.

Zhong, F.H. and Folias, E.S., "The 3D Stress Field of a Fiber Embedded into a Matrix and Subjected to an Axial Load", under review International Journal of Computational Mechanics.

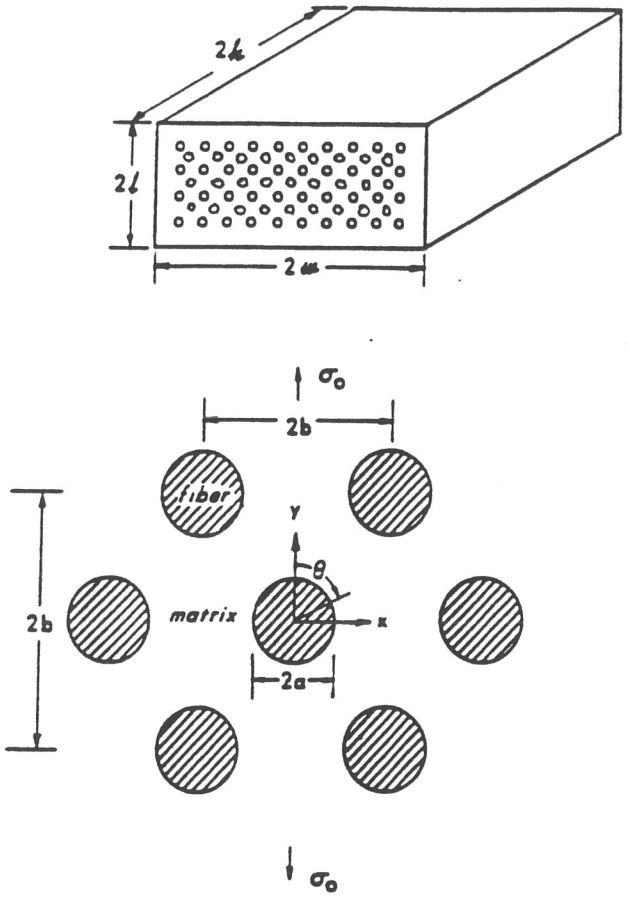

Fig. 1. Geometrical configuration

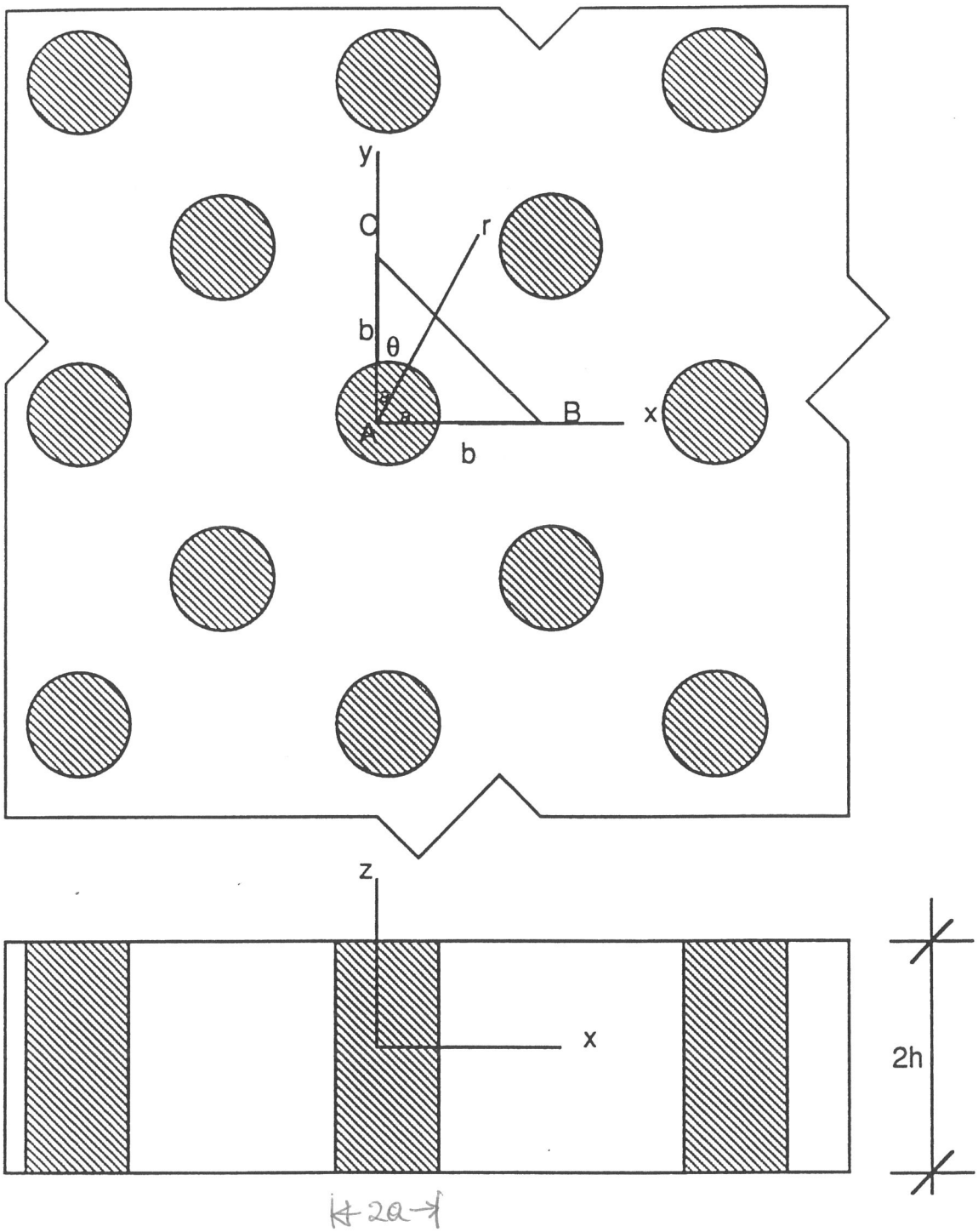

Fig. 2. Local geometrical configuration

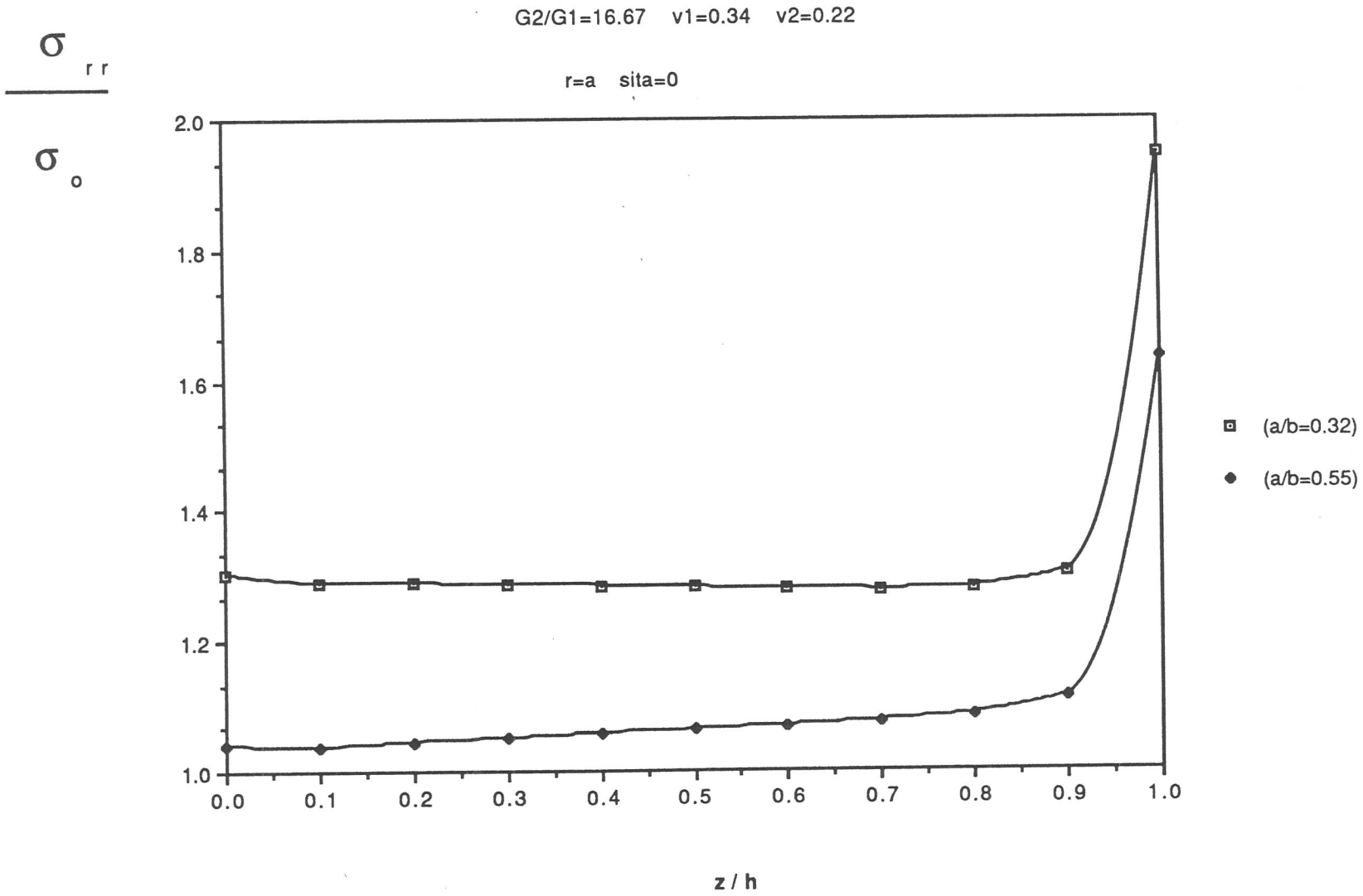

Fig. 3. Radial stress σ_{rr} versus thickness (z/h) at the position $r = a$ and $\theta = 0$.

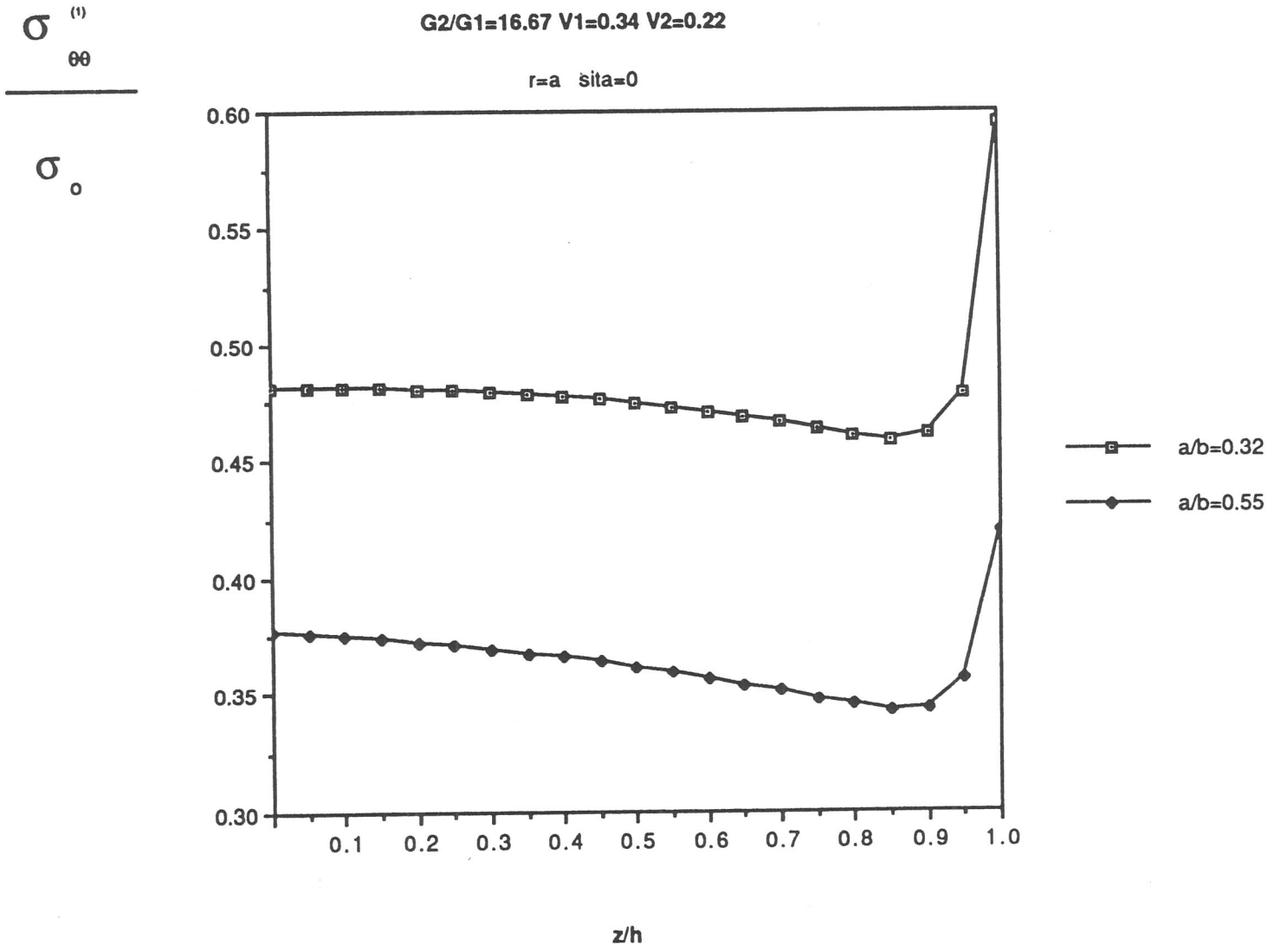

Fig. 4. Circumferential stress $\sigma_{\theta\theta}$ versus thickness (z/h), athe position $r = a$ and $\theta = \frac{\pi}{2}$

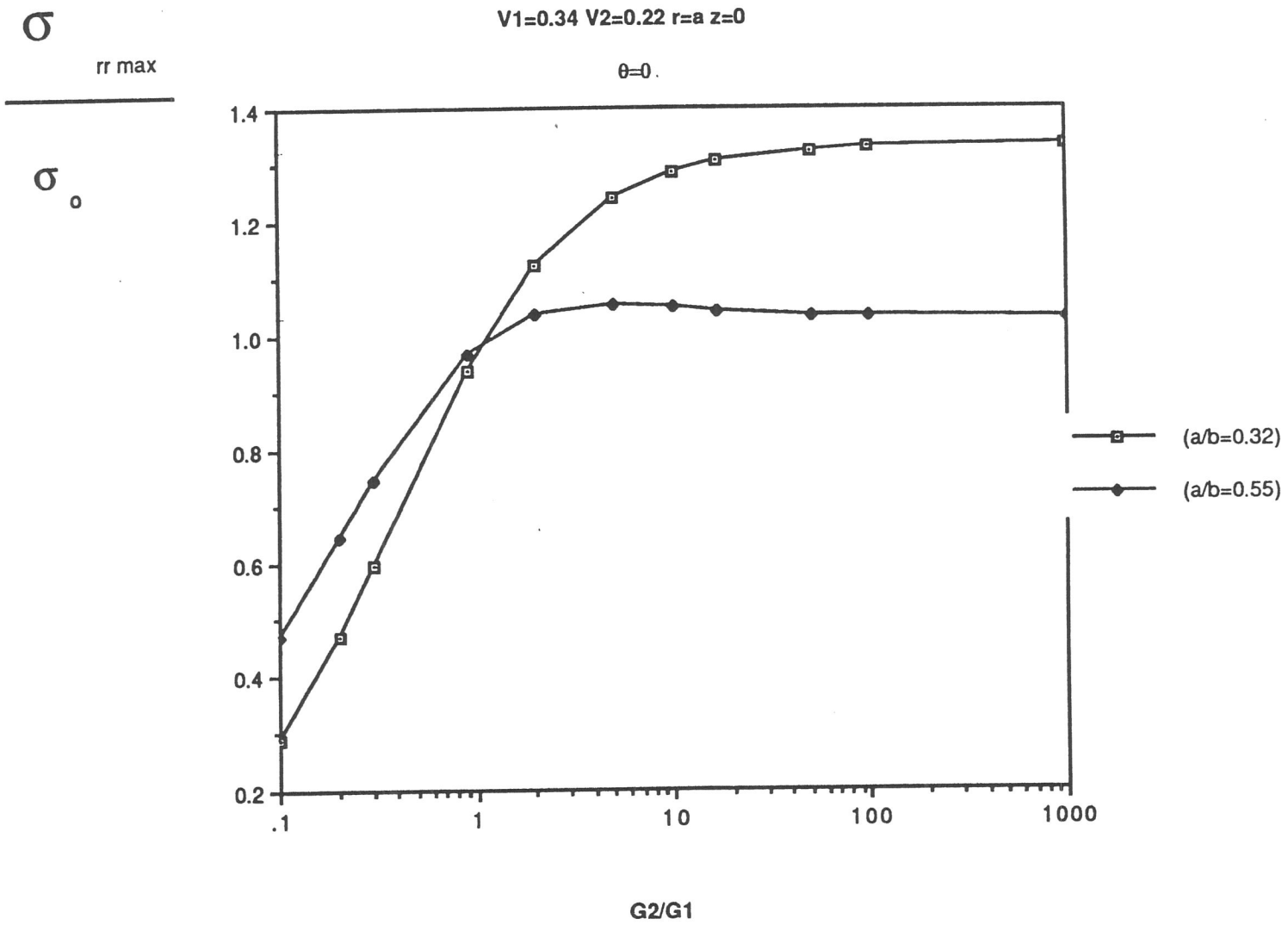

Fig. 5. Radial stress versus the ratio G_f/G_m

$\sigma^{(1)}_{\theta\theta}$

σ_o

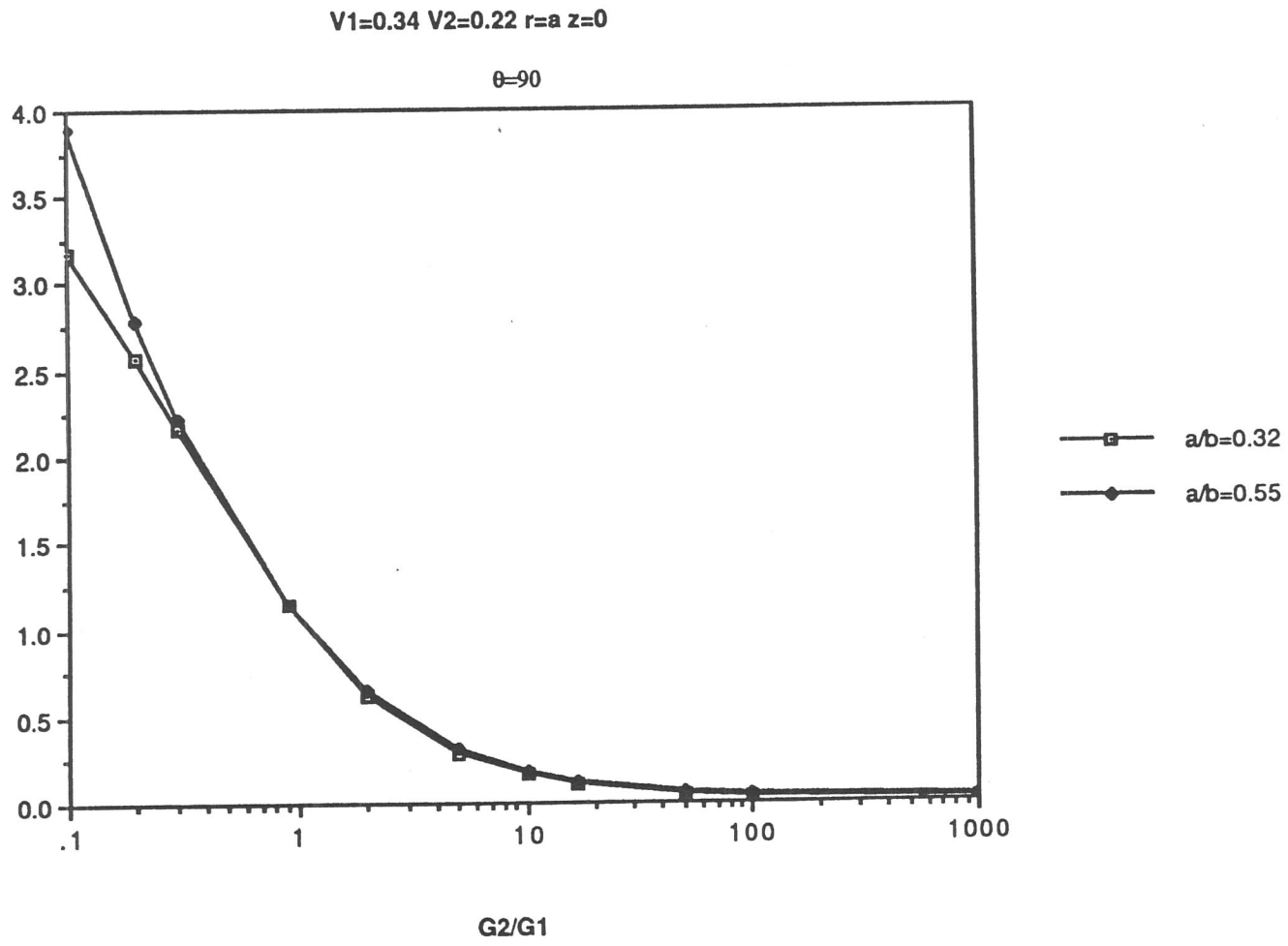

Fig. 6. Circumferential stress versus the ratio G_f/G_m.

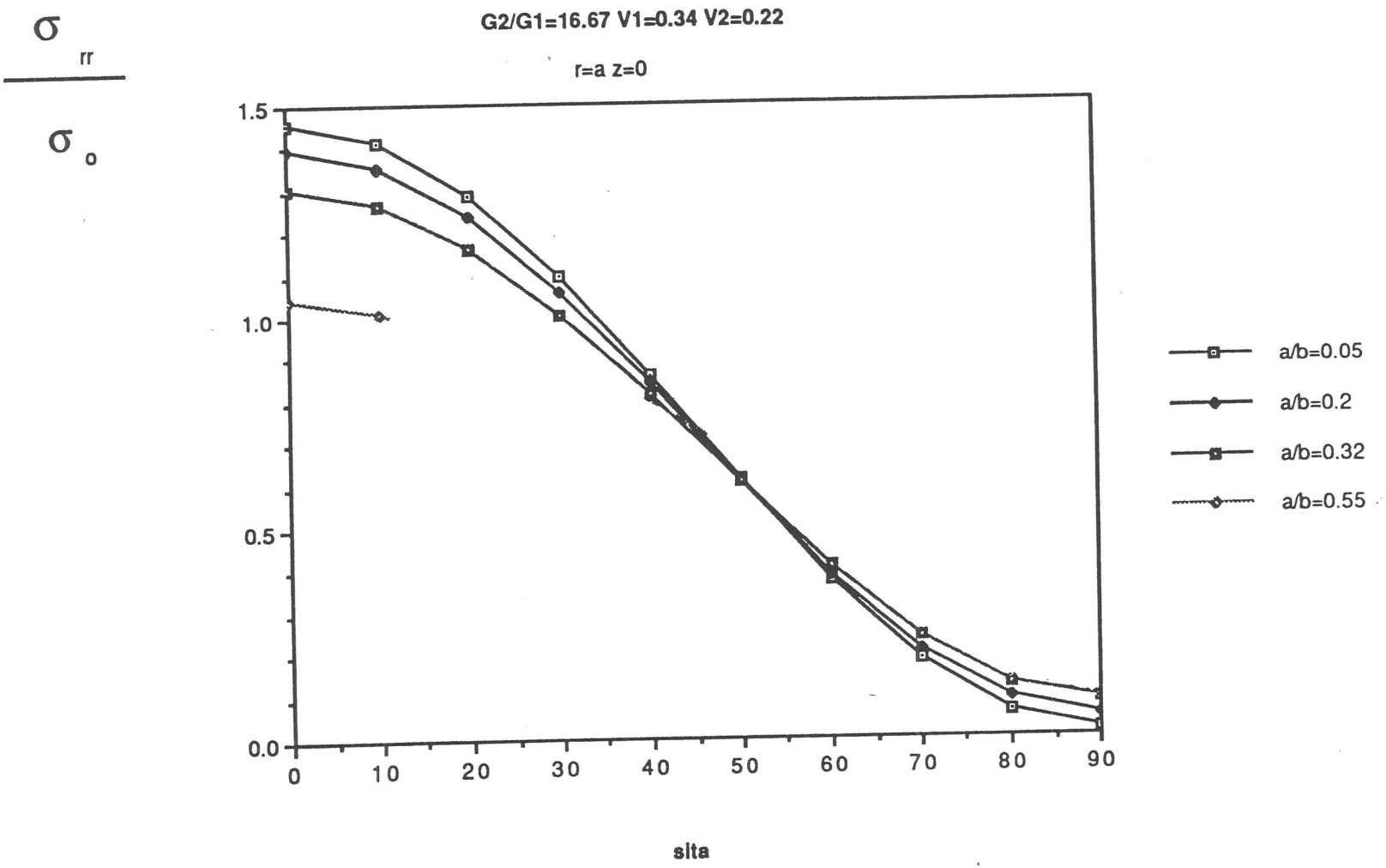

Fig. 7. Radial stress versus θ, at $r = a$.

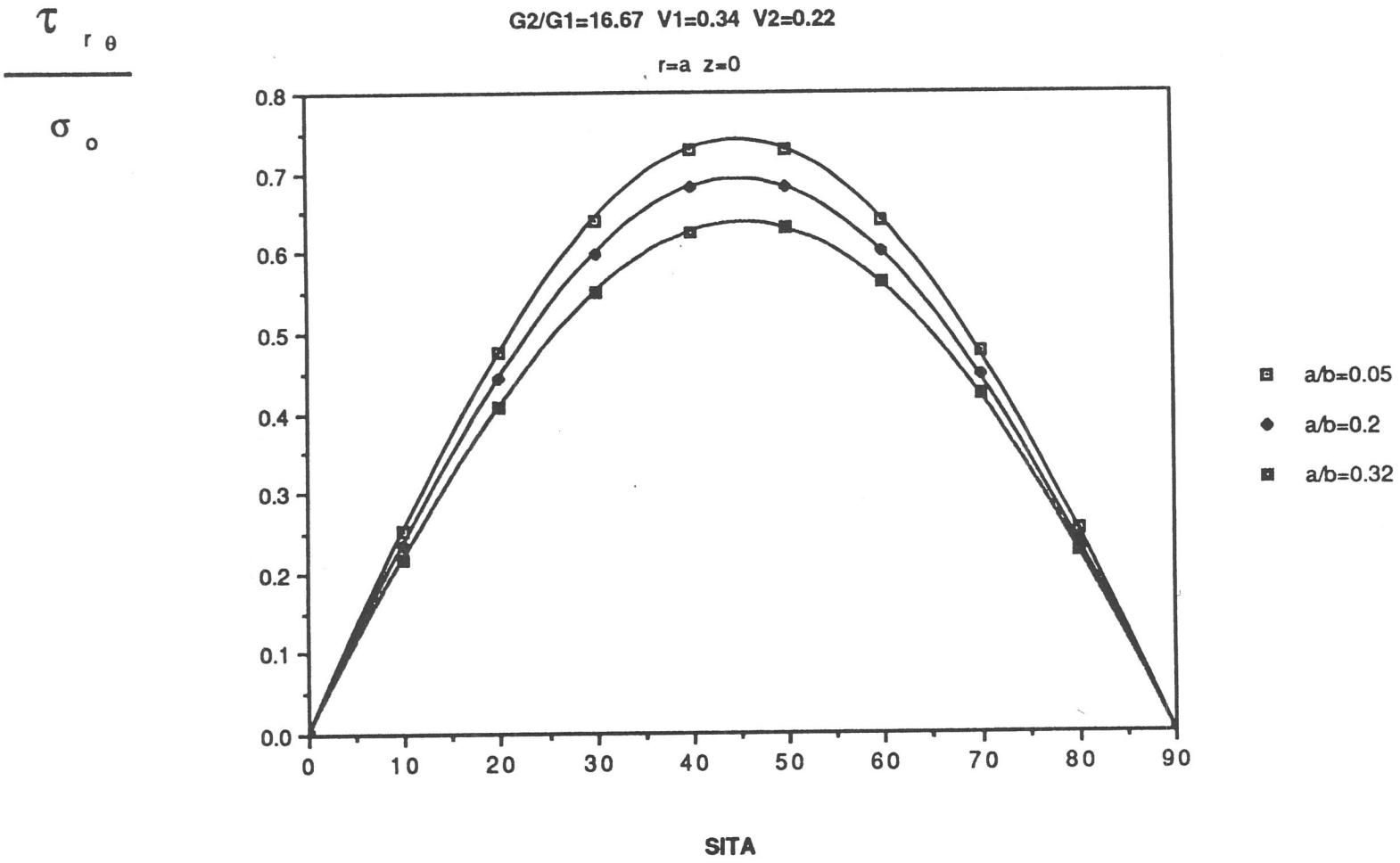

Fig. 8. Shear stress $\tau_{r\theta}$ versus θ, at $r = a$.

$\sigma_{\theta\theta}^{(1)} / \sigma_o$

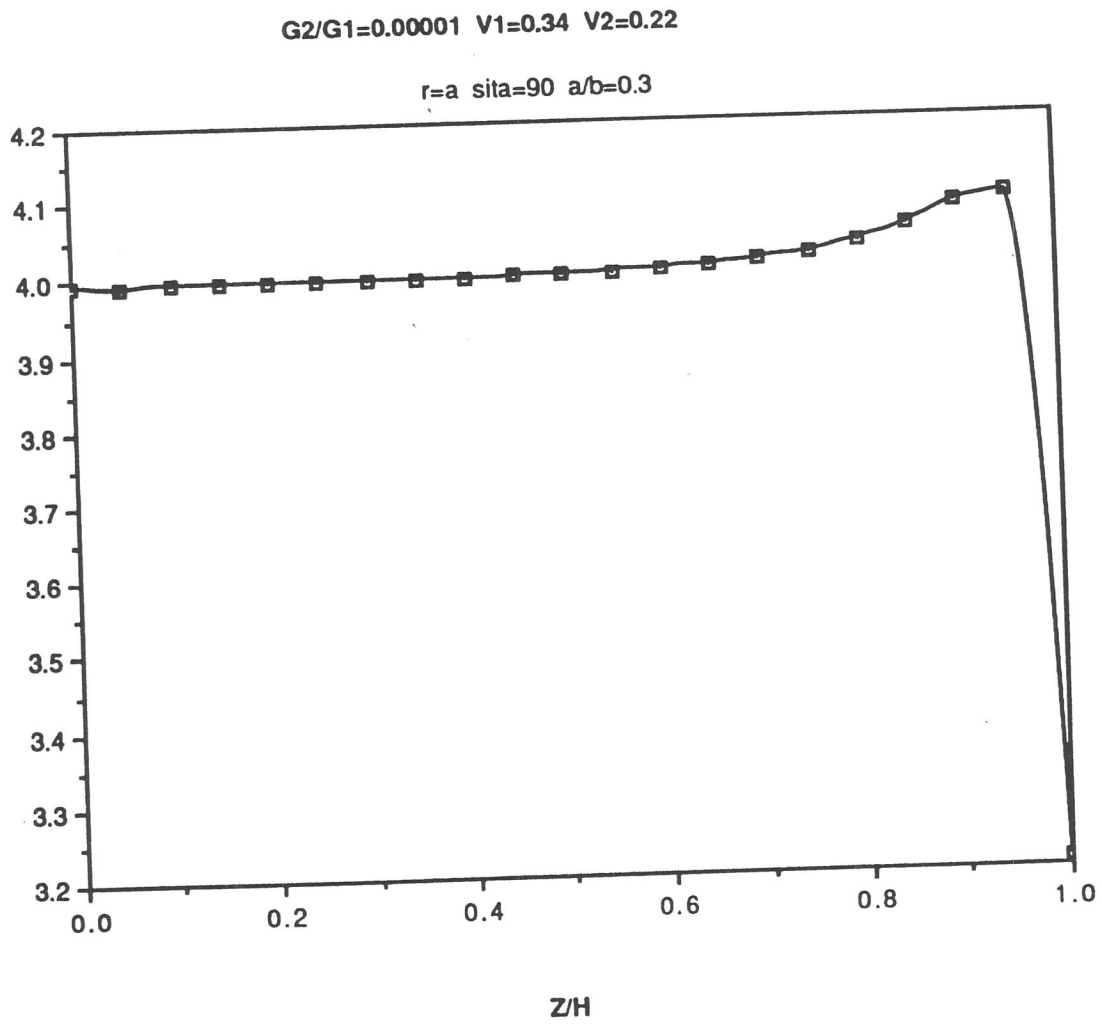

Fig. 9. The stress concentration factor versus the thickness (z/h) for a periodic array of holes.

$\sigma_{\theta\theta}^{(1)} / \sigma_o$

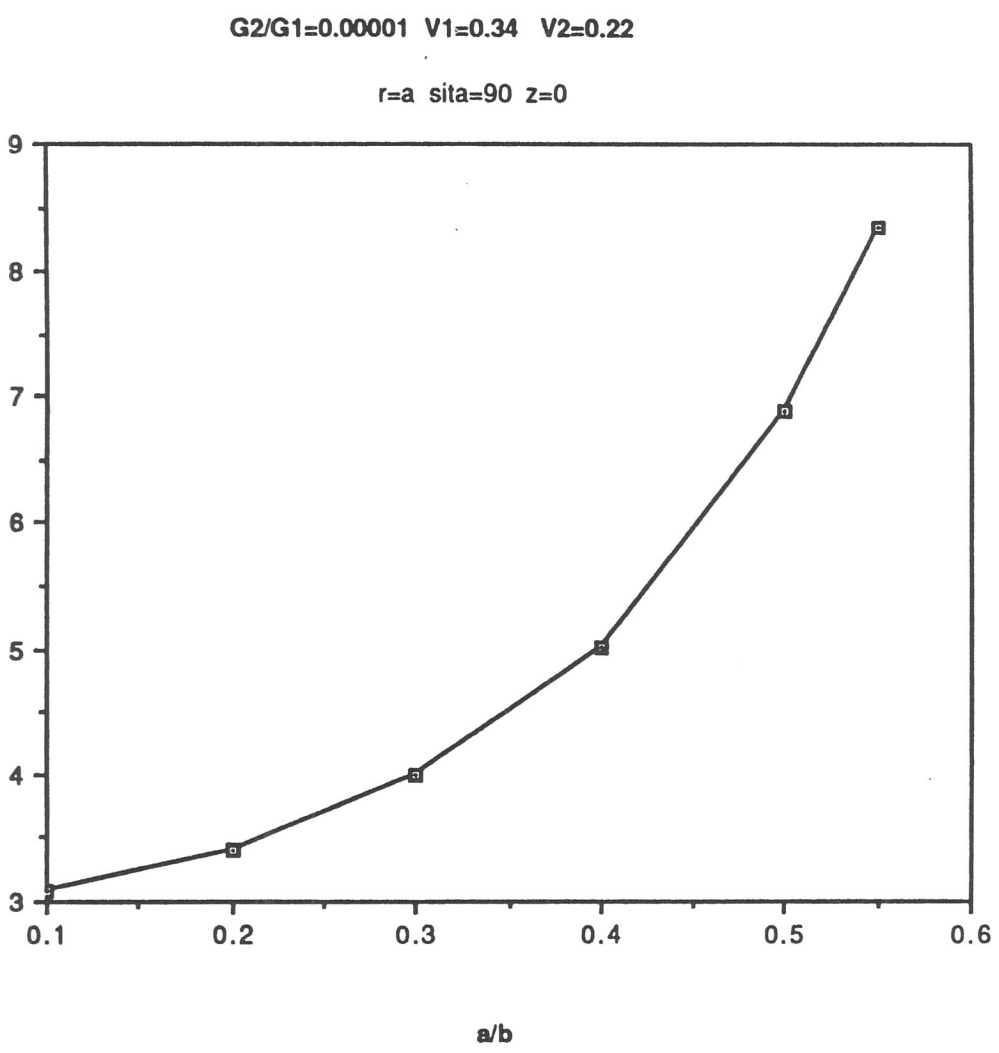

Fig. 10. The stress concentration factor versus the ratio a/b, at $z = 0$.

$\sigma^{(1)}_{\theta\theta} / \sigma_o$

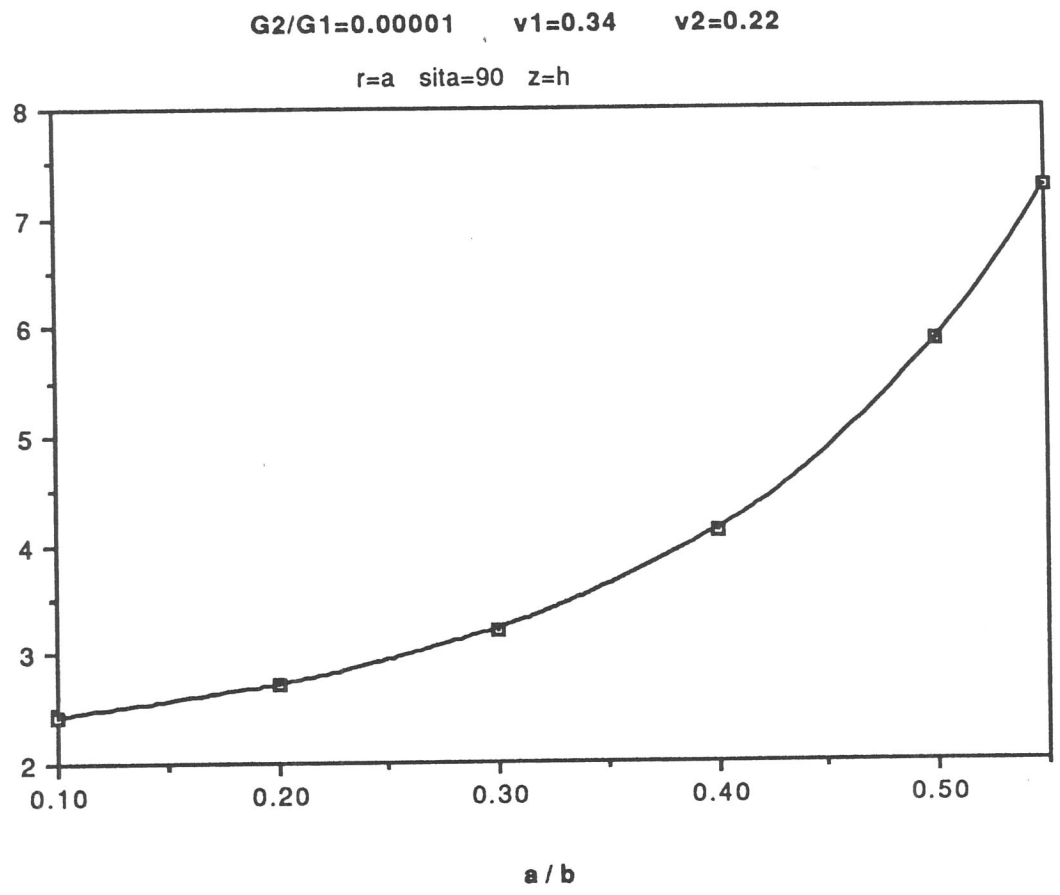

Fig. 11. The stress concentration factor versus the ratio a/b, at $z = h$.

$\sigma_{\theta\theta}^{(1)} / \sigma_o$

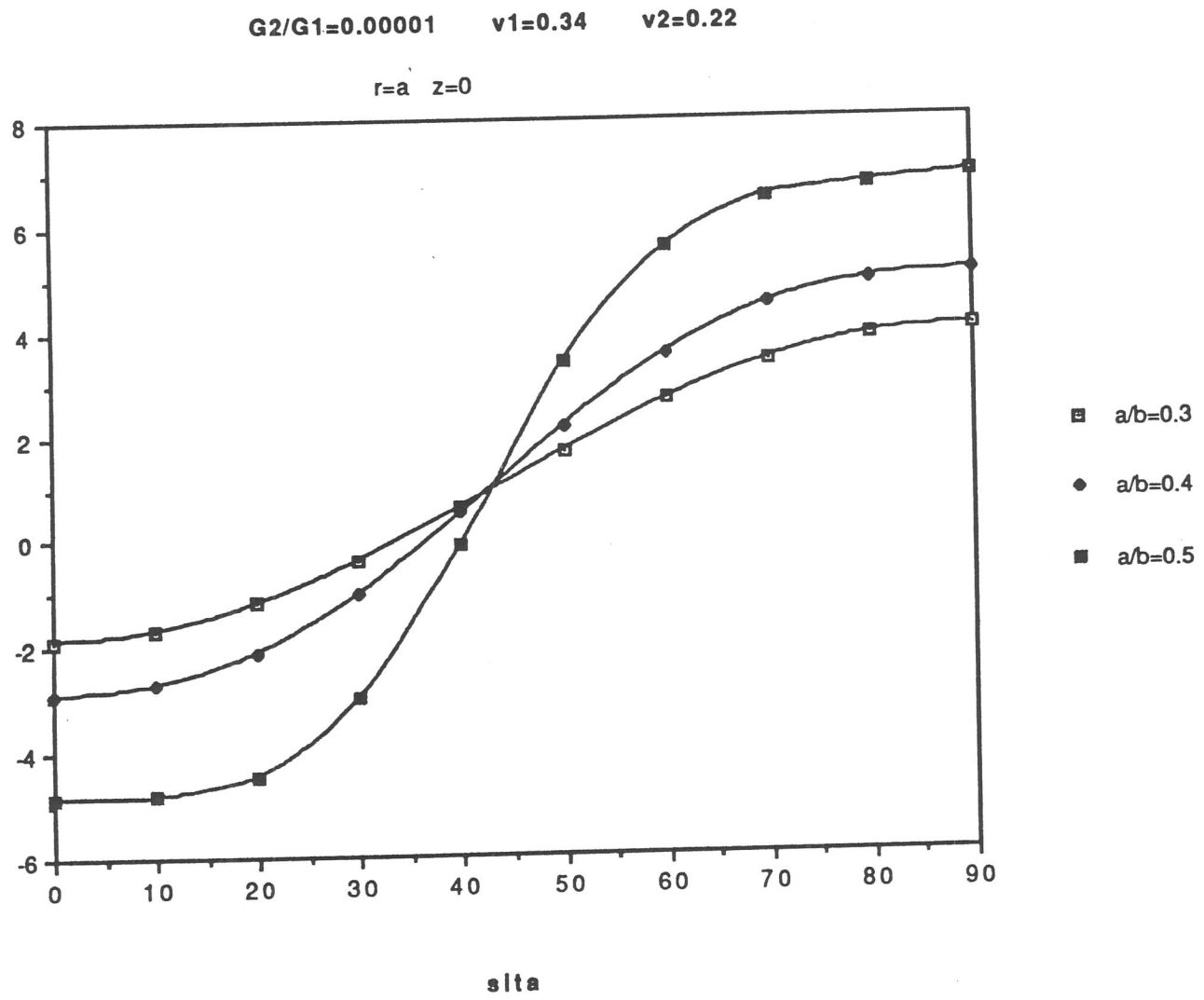

Fig. 12a. The stress concentration factor versus θ, at $z = 0$.

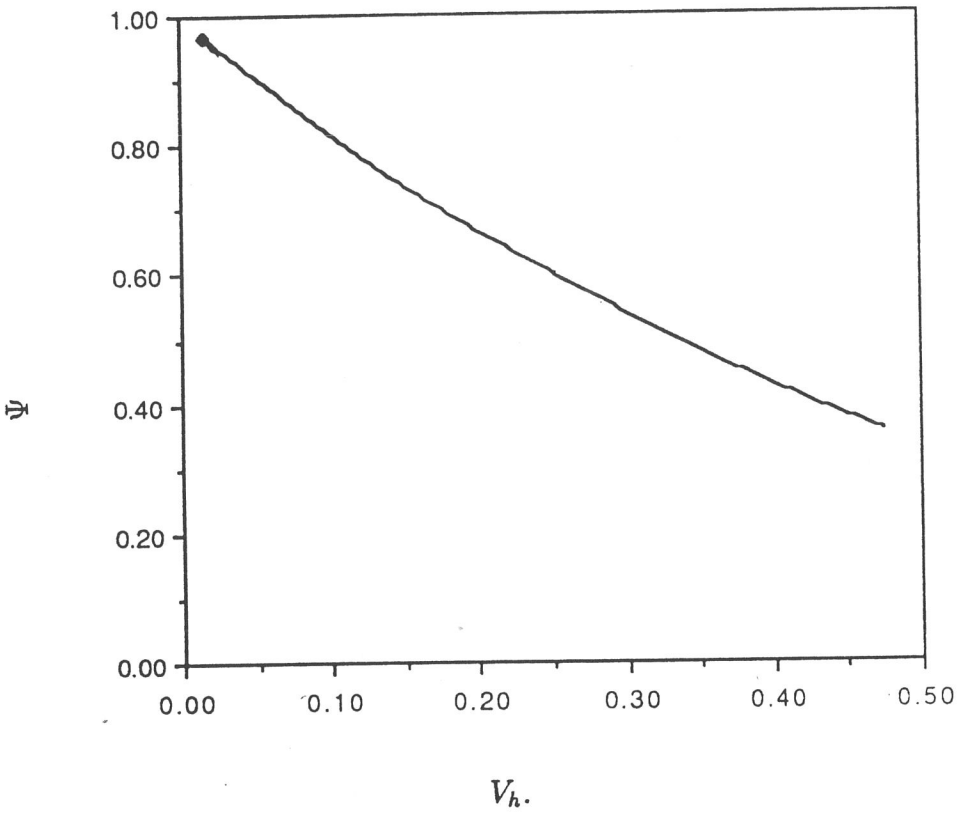

Fig. 13. The function Ψ versus the void volume ratio V_h.

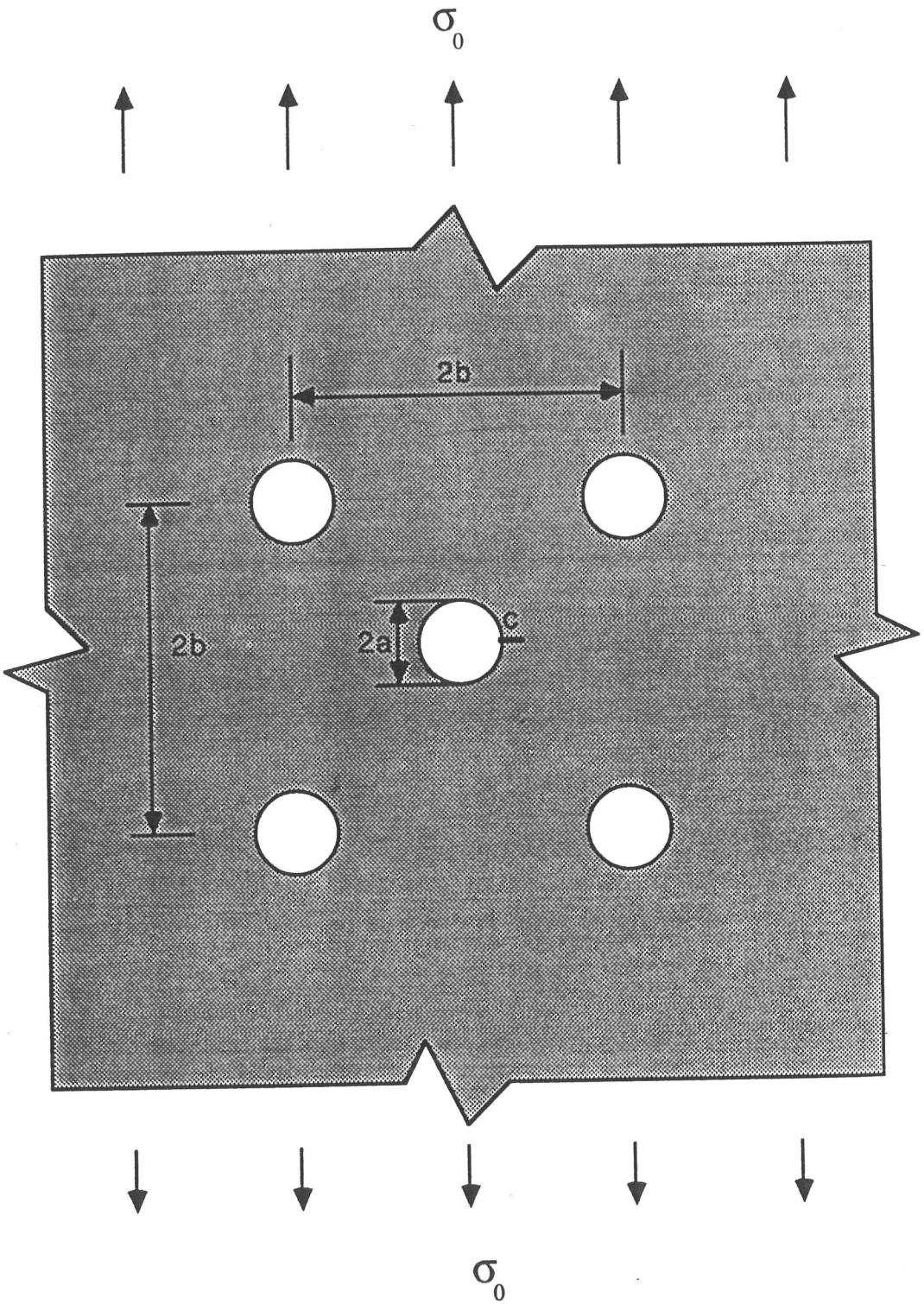

Fig 14. Plate weakened by a periodic array of holes and a small crack.